Int. J. Nonlinear Anal. Appl. 14 (2023) 1, 1093–1109
ISSN: 2008-6822 (electronic)
http://dx.doi.org/10.22075/ijnaa.2022.27473.3617

MHD stagnation point flow of Carreau nanofluid over a radially stretching sheet

G. Thirupathi[a], K. Govardhan[b], G. Narender[c,*]

[a]Department of Mathematics, Rajiv Gandhi University of Knowledge Technologies,Basar,Telangana State, India

[b]Department of Mathematics, GITAM University, Hyderabad, Telangana State, India

[c]Department of H&S (Mathematics), CVR College of Engineering, Hyderabad, Telangana State, India

(Communicated by Madjid Eshaghi Gordji)

Abstract

The numerical investigation on the flow of Carreau nanofluid past a radially stretching sheet close to a stagnation point along with convective boundary conditions has been considered. Moreover, the radiation effects and magnetic field are examined. In addition to this, the effects of heat generation/absorption are also explored. The conversion of non-linear partial differential equations describing the proposed flow problem to a set of ordinary differential equations has been carried out by employing appropriate similarity transformations. The numerical solution of the proposed flow equations is derived by the shooting method. The impact of pertinent flow parameters on the non-dimensional velocity, temperature and concentration profiles have been illustrated via tables and graphs. The limiting case of the present study affirms that the obtained numerical results reflect a very good agreement with those from open literature.

Keywords: Carreau nanofluid, heat generation/absorption, thermal radiation, MHD, Stagnation point, radially stretching sheet
2020 MSC: 35Q79

1 Introduction

Fluid serves as the necessity of life and flowing to its significance in the natural and technological processes, scientists have been discovering the various facts and figures about the fluid flow. Fluid dynamics characterizes the flow of fluids and how forces influence them. It illustrates the methodology of understanding the evolution of stars, meteorological phenomena, marine currents as well as the blood circulation. Archimedes was a Greek mathematician, who first examined the statics and buoyancy of the fluid and formulated the Archimedes principle, which was the first contribution in fluid mechanics. Rapid investigation on this subject began in the fifteenth century. Some crucial engineering applications of fluid dynamics comprise of oil pipelines, rocket engines, air conditioning systems and wind turbines.

Nanofluids are processed by the diffusion of the suspended nanoparticles in the immersed liquid (a base fluid and nanoparticles). Moreover, such fluids when compared with the conventional heat transfer fluids, have much higher rate

*Corresponding author
Email addresses: g.thirupathi8519@gmail.com (G. Thirupathi), govardhan_kmtm@yahoo.co.in (K. Govardhan), gnriimc@gmail.com (G. Narender)

Received: July 2021 *Accepted:* August 2021

of the thermal conduction and exhibit significant characteristics. Owing to their enhanced features, nanofluids have immense applications in the automobile industries, medical arena, power plant cooling systems, nuclear engineering and a lot more. Moreover, several research studies have been performed by considering the different aspects of the flows past a stretching sheet. Choi in [3] has used the term nanofluid for the first time, which is the colloidal mixture of nanoparticles and base fluid. Most of the research has shown that metallic particles transfer more heat energy as compared to non-metallic particles.

Furthermore, other types of fluids have been used for describing the different flow problems, which are not non-Newtonian in nature and are regarded as Newtonian fluids. The Carreau fluid can be regarded as a generalization of the Newtonian fluid. The analysis of the peristaltic flow [3]]-[[8] using Carreau fluid has been the field of focus of numerous researchers because of its usefulness in the scientific and technological fields, neurological and cancer treatment and Physiology. Furthermore, the stagnation point MHD flow in the light of thermal radiation for Carreau fluid has been discussed by Suneetha et al. [19]. Moreover, numerous significant aspects of the different flow problems using Carreau fluid have been discussed by a number of authors [18]-[13].

MHD is the abbreviation of magneto-hydrodynamics, in which the study of electrically active flows like plasma, liquid metals and saltwater are studied with induced magnetic field effects (external or internal) [6]. Many researches have already carried out in studying the role of MHD effects for the improvement of heat transport mechanism. In the past few years, the problem involving stagnation point flow has acquired the considerable attention of many research scientists.

In the past few years, the problem involving stagnation point flow has acquired the considerable attention of many research scientists. Owing to its significant properties, the study of flow nearby a stagnation point past a stretching/shrinking sheet has a wide range of practical applications, for instance, cooling process of atomic reactors and electronic equipment, the layouts of thrust bearings, and several hydrodynamics processes. Moreover, the analysis of the magnetohydrodynamics flow is highly significant in the fluid dynamics flowing to the reason that the impact of the magnetic field on the viscous flow using a fluid having electrically conducting properties has played a key role in several commercial production, for instance in the refinement of crude oil, glass and paper production, manufacturing of magnetic materials, geophysics and MHD electrical power generation. The MHD factor has a fundamental role to play in controlling the cooling rate and for achieving the desired quality of the product. Mahapatra [14] analyzed the flow nearby a stagnation point by taking into consideration the heat transfer past a stretching sheet. Furthermore, Nazar et al. [16] discussed the stagnation point flow over a stretching sheet using a micro polar fluid. Several researchers have contributed in the study of the stagnation point MHD flow in the light of various significant effects [17]-[15].

Moreover, an analysis of the flow using the radially stretching surfaces for the nanofluids, has many significant applications in the industrial sectors, for instance, drawing of plastic films, manufacturing of glass, production of paper and refining of crude oil. In addition to this, the implementation of the nano technology has been an aim of the recent analysis by many scholars because the nanoparticles exhibit remarkable electrical, optical, chemical behavior and due to their Brownian motion and thermophoresis properties. Owing to such features, the nanoparticles are widely used in catalysis, imaging, energy-based research, microelectronics, medical and environmental applications. These particles are composed of metals or non-metals. On top of that, latest investigations have made the in- fusion of nanoparticles, practicable in heat transfer fluids most notably water, diethylene glycol and propylene glycol to convert them into a more efficient category of heat transfer fluids.

Motivated by the formerly findings on the non-Newtonian and Newtonian fluids, the study of stagnation point MHD flow using the Carreau nanofluids has been presented.

2 Problem Statement

The physical model under study is represented in Figure [1] Two dimensional,steady, and incompressible flow is investigated. The coordinate system is chosen in such a way that $r-$ axis is along the flow whereas $z-$ axis is perpendicular to the flow. The velocity of the outer flow is taken as U_e . Furthermore, the direction of the uniform magnetic field is chosen in such a manner that it is normal to the surface of the fluid flow. The effects of Brownian motion and thermophoresis have been elaborated. Moreover, the convective surface conditions have been taken into consideration.

2.1 The Governing Equations

Two-dimensional system of governing equations consisting of continuity, momentum, energy and concentration is [12]

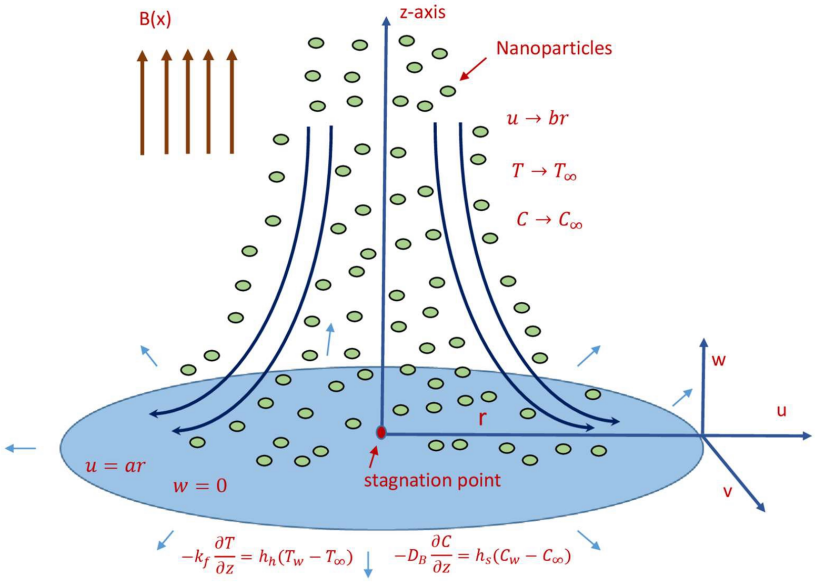

Figure 1: Schematic of physical model.

$$\frac{\partial u}{\partial r} + \frac{u}{r} + \frac{\partial w}{\partial z} = 0 \tag{2.1}$$

$$\frac{\partial u}{\partial r}u + \frac{\partial u}{\partial z}w = -\frac{\sigma B_0}{\rho_f}(u - U_e) + U_e\left(\frac{dU_e}{dr}\right) + v_f(n-1)\Gamma^2\left(\frac{\partial^2 u}{\partial r^2} + \frac{\partial^2 u}{\partial z^2}\right)\left(\frac{\partial u}{\partial z}\right)^2\left(1 + \Gamma^2\left(\frac{\partial u}{\partial z}\right)^2\right)^{\frac{n-3}{2}} + v_f\left(\frac{\partial^2 u}{\partial r^2} + \frac{\partial^2 u}{\partial z^2}\right)\left[1 + \Gamma^2\left(\frac{\partial u}{\partial z}\right)^2\right]^{\frac{n-1}{2}} \tag{2.2}$$

$$\frac{\partial T}{\partial r}u + \frac{\partial T}{\partial z}w = -\frac{v_f}{\rho_p}\left(1 + \frac{1}{\beta}\right)\left(\frac{\partial u}{\partial z}\right)^2 + \alpha_f\left(\frac{\partial^2 T}{\partial r^2} + \frac{\partial^2 T}{\partial z^2}\right) - \frac{1}{(\rho c_p)_f}\left(\frac{\partial q_r}{\partial z}\right) + \tau\left[D_B\left(\frac{\partial C}{\partial z}\frac{\partial T}{\partial z} + \frac{\partial C}{\partial r}\frac{\partial T}{\partial r}\right) + \frac{D_T}{T_\infty}\left(\frac{\partial T}{\partial r}\right)^2 + \left(\frac{\partial T}{\partial z}\right)^2\right] + \frac{Q_0}{(\rho c_p)_f(T - T_\infty)} + \frac{\rho B_0^2(u - U_e)^2}{(\rho c_p)_f} \tag{2.3}$$

$$\frac{\partial C}{\partial r}u + \frac{\partial C}{\partial z}w = D_B\left(\frac{\partial^2 C}{\partial r^2} + \frac{\partial^2 C}{\partial z^2}\right) - \frac{D_T}{T_\infty}\left(\frac{\partial^2 T}{\partial r^2} + \frac{\partial^2 T}{\partial z^2}\right) - C_r(C - C_\infty) \tag{2.4}$$

2.2 The Dimension form of the Boundary Conditions

$$u = U_w(r) = ar,\ w = 0,\ -k_f\frac{\partial T}{\partial z} = h_h(T_f - T),\ -D_B\frac{\partial C}{\partial z} = h_s(C_f - C)\ at\ z = 0$$

$$u \to U_s = br, T \to T_\infty, C \to C_\infty \text{ as } z \to \infty. \tag{2.5}$$

2.3 The Dimensionless Governing Equations

The following process was implemented to convert the PDEs to ODEs:

$$\eta = z\sqrt{\frac{a}{v_f}},\ u = ar\,f'(\eta),\ w = -2\sqrt{av_f}f(\eta),\ \theta(\eta) = \frac{T - T_\infty}{T_f - T_\infty},\ \phi(\eta) = \frac{C - C_\infty}{C_w - C_\infty} \tag{2.6}$$

The Rosseland approximation has been considered for the radiation. For smaller value of temperature contrast, the temperature difference T^4 might be expanded about T_∞ using Taylor series and ignoring the higher order terms, the formula for the radiative heat flux q_r is stated below.

$$\frac{\partial q_r}{\partial z} = -\frac{16\sigma^* {T_\infty}^3}{3k^*}\frac{\partial^2 T}{\partial z^2} \tag{2.7}$$

Under the above circumstances, the governing system in non dimensional form can be expressed as

$$\left(1+nWe^2\left(f''\right)^2\right)\left(\left(1+We^2\left(f''\right)^2\right)^{\frac{n-3}{2}} f''' + 2ff'' - \left(f'\right)^2 + A^2 - M^2\left(f'-A\right) = 0 \tag{2.8}$$

$$\left(1+\frac{4}{3}R\right)\theta'' + \Pr\left(f\theta' + Nb\phi'\theta' + Nt\left(\theta^1\right)^2 + Ec\left(f'\right)^2 + Q\theta + EcM^2\left(f'-A\right)^2\right) = 0 \tag{2.9}$$

$$\phi'' + Sc\left(2f\phi' - \gamma\phi\right) + \frac{Nt}{Nb}\theta'' = 0 \tag{2.10}$$

The boundary condition in dimensionless form

$$\left.\begin{array}{l} f(0)=0,\ f'(0)=1,\ \theta'(0)=-Bi_1[1-\theta(0)],\ \phi'(0)=-Bi_2\left[1-\phi(0)\right]\ as\ \eta=0 \\ f'(\infty)\to A,\ \theta(\infty)\to 0,\ \phi(\infty)\to 0 \text{ as } \eta\to\infty \end{array}\right\} \tag{2.11}$$

The dimensionless parameters are defined as

$$\left.\begin{array}{lll} Nb=\dfrac{\tau D_B(C_f-C_\infty)}{v_f}, & Pr=\dfrac{v_f}{\alpha}, & Nt=\dfrac{\tau D_T(T_f-T_\infty)}{v_f T_\infty}, \quad M^2=\dfrac{\sigma B_0^2}{\rho a}, \\ Q=\dfrac{Q_0}{\rho c_p a}, & R=\dfrac{4T_\infty\rho^*}{k^*(\alpha\rho c_p)}, & Ec=\dfrac{a^2r^2}{\alpha c_p(T_f-T_\infty)}, \quad A=\dfrac{b}{a}, \\ Sc=\dfrac{v_f}{D_B}, & \gamma=\dfrac{C_r}{a}, & Bi1=\dfrac{h_h}{k_f}\sqrt{\dfrac{v_f}{a}}, \quad Bi2=\dfrac{h_s}{D_B}\sqrt{\dfrac{v_f}{a}} \end{array}\right\} \tag{2.12}$$

The surface drag coefficient, is obtained as:

$$\begin{aligned} C_f &= \frac{\tau_w}{\rho_f U_w^2} = \frac{\mu\left(1+\Gamma^2\left(\frac{\partial u}{\partial z}\right)^2\right)^{\frac{n-1}{2}}\left(\frac{\partial u}{\partial z}\right)_{z=0}}{\rho_f U_w^2} \\ \Rightarrow C_f Re^{\frac{1}{2}} &= -f''(0)\left[1+We^2 f''^2(0)\right]^{\frac{n-1}{2}}. \quad \left(\because Re=\frac{rU_w}{v_f}\right) \end{aligned} \tag{2.13}$$

The local heat transfer number is given as:

$$\begin{aligned} Nu &= \frac{rq_w}{k_f\left(T_f-T_\infty\right)} = \frac{-k_f r\left(\frac{\partial T}{\partial z}-\frac{q_r}{k_f}\right)_{z=0}}{k_f\left(T_f-T_\infty\right)} \\ \Rightarrow NuRe^{-\frac{1}{2}} &= -\left[1+\frac{4}{3}R\right]-\theta'(0). \end{aligned} \tag{2.14}$$

The nearby mass exchange number is given as:

$$\begin{aligned} Sh &= \frac{rq_m}{D_B\left(\phi_f-\phi_\infty\right)} = \frac{-D_B r\left(\frac{\partial C}{\partial z}\right)_{z=0}}{D_B(\phi_f-\phi_\infty)} \\ \Rightarrow ShRe^{-\frac{1}{2}} &= -\phi'(0). \end{aligned} \tag{2.15}$$

3 Solution Methodology

To solve the differential equations (2.8)-(2.10), the shooting technique has been used. Since, equation (2.8) involves only and its derivatives, it can be solved separately by the shooting. The solution of equation (2.8) will be used in

equation (2.9) and equation (2.10) as a known input.

It can be observed that for the third order ODE equation (2.8), two initial conditions are given at $\eta = 0$. Let us denote the missing initial condition f'' by r . For further proceeding, the following notations have been introduced.

$$f = h_1, \quad f' = h_2, \quad f'' = h_3, \quad \frac{\partial f}{\partial r} = h_4, \quad \frac{\partial f'}{\partial r} = h_5, \quad \frac{\partial f''}{\partial r} = h_6 \tag{3.1}$$

Utilizing the above notations, one can effectively have the taking after system of first order ODEs:

$$\left.\begin{array}{ll} h_1' = h_2, & h_1(0) = 0, \\ h_2' = h_3, & h_2(0) = 1, \\ h_3' = \dfrac{\left[h_2^2 + M^2\left(h_2 - A\right) - 2h_1h_3 - A^2\right]}{\left(1 + nWe^2h_3^2\right)\left(1 + We^2h_3^2\right)^{\frac{n-3}{2}}}, & h_3(0) = r, \\ h_4' = h_5, & h_4(0) = 0, \\ h_5' = h_6, & h_5(0) = 0, \\ h_6' = \dfrac{1}{\left(1 + nWe^2h_3^2\right)^2\left(1 + We^2h_3^2\right)^{n-3}} \begin{pmatrix} \left(1 + nWe^2h_3^2\right)\left(1 + We^2h_3^2\right)^{\frac{n-3}{2}} \\ \left[\left(2h_2 + M^2\right)h_5 - 2\left(h_1h_6 + h_3h_4\right)\right] \\ -\left(h_2^2 + M^2\left(h_2 - A\right) - 2h_1h_3 - A^2\right) \\ \left[1 + We^2h_3^2\right]^{\frac{n-5}{3}}\left(2We^2h_3h_6\right) \\ \left(\frac{n-3}{2}\left[1 + nWe^2h_3^2\right] + n\left(1 + We^2h_3^2\right)^{-1}\right) \end{pmatrix}, & h_6(0) = 1 \end{array}\right\} \tag{3.2}$$

The above initial value problem (IVP) will be solved numerically by using shooting technique along with Adams-Moulton method. To implement the Adams-Moulton method, the missing initial condition will be chosen as $r = r_0$. For the refinement of the missing condition, Newton's method for root finding has been used which is governed by the following iterative formula:

$$\begin{aligned} r^{(n+1)} &= r^{(n)} - \frac{\left(h_2\left(\eta_\infty\right)\right)_{r=r^{(n)}} - 1}{\left(\frac{\partial h_2(\eta_\infty)}{\partial r}\right)_{r=r^{(n)}}} \\ \Rightarrow r^{(n+1)} &= r^{(n)} - \frac{\left(h_2(\eta_\infty)\right)_{r=r^{(n)}} - A}{\left(h_2\left(\eta_\infty\right)\right)_{r=r^{(n)}}} \end{aligned} \tag{3.3}$$

For numerical solution of equation (2.8), the unbounded space $[0, \infty]$ has been supplanted by a bounded space $[0, \eta_\infty]$ where η_∞ is a positive number such that the variation in solution for $\eta > \eta_\infty$ is ignorable. the execution of the Newton's method can be presented in the following algorithmic form:

Step-1: Choose an initial guess $r = r_0$ in the equation (2.8) and solve it by the Adams- Moulton Method.

Step-2: If for a very small positive number ϵ ,

$$\mid h_2(r^k)_{\eta=\eta_\infty} - A \mid > \epsilon, for\ k = 0, 1, 2... \tag{3.4}$$

then go to Step-3, otherwise the solution is there.

Step-3: Compute the next value of the missing initial condition $r^{k+1}; k = 0, 1, 2...$ by using the Newton's scheme given by (3.3).

Step-4: Repeat Step-1 with $r = r^{k+1}$.

Now to solve equations (2.9) and (2.10) numerically, the missing initial conditions $\theta(0) = 0$ and $\phi(0)$ have been denoted by s and t , respectively. Thereby the following notations have been considered.

$$\left.\begin{array}{l} \theta = y_1,\ \theta' = y_2,\ \phi' = y_3,\ \phi'' = y_4,\ \dfrac{\partial\theta}{\partial l} = y_5,\ \dfrac{\partial\theta'}{\partial l} = y_6,\ \dfrac{\partial\phi}{\partial l} = y_7 \\ \dfrac{\partial\phi'}{\partial l} = y_8,\ \dfrac{\partial\theta}{\partial m} = y_9,\ \dfrac{\partial\theta'}{\partial m} = y_{10},\ \dfrac{\partial\phi}{\partial m} = y_{11},\ \dfrac{\partial\phi'}{\partial m} = y_{12} \end{array}\right\} \tag{3.5}$$

The above mathematical model (2.9)-(2.10), can now be listed in the form of the following first order coupled

ODEs.

$$\left.\begin{array}{ll}
y_1 = y_2, & y_1(0) = s, \\
y_2' = \dfrac{-3}{3+4R}\left(\begin{array}{l}\Pr Nby_2y_4 + \Pr Nty_2^2 + 2\Pr h_1y_2 + \Pr Qy_1 \\ +\left(1+\frac{1}{\beta}\right)\Pr Ech_3^2 + +\Pr EcM^2\left(h_2-A\right)^2\end{array}\right), & y_2(0) = -Bi_1(1-s), \\
y_3' = y_4, & y_3(0) = t, \\
y_4' = -\left(\dfrac{Nt}{Nb}\right)y_2' - Sc\left(2h_1y_4 - \gamma y_3\right), & y_4(0) = -Bi_2(1-t), \\
y_5' = y_6, & y_5(0) = 1, \\
y_6' = \dfrac{-3\Pr}{3+4R}\left(\left(Nby_4 + 2Nty_2 + 2h_1\right)y_6 + Nby_2y_8 + By_5\right), & y_6(0) = Bi_1, \\
y_7' = y_8, & y_7(0) = 0, \\
y_8' = \dfrac{3Nt\Pr}{Nb(3+4R)}\left(\begin{array}{l}\left(Nby_4 + 2Nty_2 + 2h_1\right)y_6 + By_5 + Nby_2y_8 \\ -2Sch_1y_8 + Sc\gamma y_7\end{array}\right), & y_8(0) = 0, \\
y_9' = y_{10}, & y_9(0) = 0, \\
y_{10}' = \dfrac{-3\Pr}{3+4R}\left(\left(Nby_4 + 2Nty_2 + 2h_1\right)y_{10} + Nby_2y_{12} + By_9\right), & y_{10}(0) = 1, \\
y_{11}' = y_{12}, & y_{11}(0) = 0, \\
y_{12}' = \dfrac{3Nt\Pr}{Nb(3+4R)}\left(\begin{array}{l}\left(Nby_4 + 2Nty_2 + 2h_1\right)y_{10} + By_9 \\ +Nby_2y_{12} - 2Sch_1y_{12} + Sc\gamma y_{11}\end{array}\right), & y_{12}(0) = 0
\end{array}\right\} \tag{3.6}$$

The Adams-Moulton method has been taken into consideration for solving the above initial value problem. In the above system of equations, the missing conditions are to be chosen such that

$$\left(y_1(\eta_\infty, s, t)\right)_{\eta=\eta_\infty} = 0, \left(y_3(\eta_\infty, s, t)\right)_{\eta=\eta_\infty} = 0 \tag{3.7}$$

For the improvement of the missing condition, Newton's method has been implemented which is conducted by the following iterative scheme:

$$\begin{bmatrix} s^{(n+1)} \\ t^{(n+1)} \end{bmatrix} = \begin{bmatrix} s^{(n)} \\ t^{(n)} \end{bmatrix} - \left[\begin{bmatrix} y_5 & y_7 \\ y_9 & y_{11} \end{bmatrix}^{-1} \begin{bmatrix} y_1 \\ y_3 \end{bmatrix}\right]_{\left(s^{(n)}, t^{n(n)}\cdot\eta_\infty\right)} \tag{3.8}$$

The following steps are involved for the accomplishment of the shooting method.
(i) Choice of the guesses $s = s_0$ and $t = t_0$.
(ii) Choice of a positive small number δ .
If max $\{\mid y_1(\eta_\infty - 0)\mid, \mid y_3(\eta_\infty - 0)\mid\} < \delta$, stop the process otherwise go to (iii).
(iii) Compute $s^{k+1}$and $t^{k+1}; k = 0, 1, 2, 3, 4....$ by using (3.8).
(iv) Repeat (i) and (ii). In a similar manner, the ODEs (9-10) along with the associated BCs can be solved by considering f as a known function.

4 Representation of Graphs and Tables

In this area the numerical comes about have been appeared within the frame of graphs and table. The effect of a few parameters on speed f' temperature θ and concentration ϕ have been studied.

Dianchen et al. [12] used the RK method for the numerical solution of the discussed model. In the present survey, the shooting method has been opted for reproducing the solution of [12].The results discussed in Table [1], illustrates the impacts of significant parameters on the skin friction coefficients $-C_fRe^{\frac{1}{2}}$. The results are compared with those of Dianchen et al. [12] showing an excellent agreement. For the rising values of the M skin friction coefficients increases.

Tables [1]-[3] disclose the numerical results of skin-friction coefficient, Nusselt and Sherwood numbers for the present model regarding a change in the values of various parameters like n, We, M, R, A, Pr, Q, Nb, Nt, Ec, Sc, γ, $Bi1$ and $Bi2$.

For the larger values of n and A , the skin-friction coefficient depresses whereas the heat and mass transfer rates climb marginally. The skin-friction coefficient, Nusselt and Sherwood numbers are enhanced as We assumes the higher

values. A rise in the value of M depreciates the Nusselt number whereas the skin-friction coefficient and Sherwood number increase significantly.Both the Nusselt and Sherwood numbers increase with an escalation in the value of R,Sc and γ. As the value of Q,Pr and $Bi1$ rise, the Nusselt number is enhanced whereas the Sherwood number shows a declining behavior. A decrement in the heat and mass transfer rates has been observed for the higher estimation of Nb,Ec and $Bi2$, the heat transfer rate falls, however, the mass transfer rate rises.

Table 1: Comparison of the present results of $f''(0)$ with those presented by Dianchen et al. [12].

$f''(0)$ with $We = 0, n = 1$

M	**Dianchen et al.[12]**	**Present**
0.0	-1.173720	-1.173734000
0.5	-1.365814	-1.365818000
1.0	-1.535709	-1.535711000
2.0	-1.830490	-1.830479000
3.0	-2.084846	-2.084804000

Table 2: The computed results of skin-friction coefficient, Nusselt and Sherwood numbers for $\gamma = 1$, $Bi1 = 0.1 = Bi2$, where a_1=$(1 + We^2 f''^2(0))^{\frac{n-1}{2}}$ and a_2=$(1 + \frac{4}{3}R)$.

n	**W**e	**A**	**M**	**R**	**P**r	**N**b	**N**t	**Q**	$-\mathbf{a_1 f''(0)}$	$-\mathbf{a_2}\theta'(\mathbf{0})$	$\phi'(\mathbf{0})$
1.5	0.05	0.1	1.0	0.1	0.7	0.5	0.1	0.1	1.433997000	0.098130110	0.093177580
2.0									1.433127000	0.098129110	0.093177860
2.5									1.432260000	0.098128130	0.093178140
	0.5								1.475784000	0.098024100	0.093209210
	1.0								1.551808000	0.097877640	0.093259680
		0.2							1.318361000	0.098848320	0.093254310
		0.3							1.190385000	0.099152530	0.093339640
			1.2						1.551992000	0.097290090	0.093161700
			1.4						1.681274000	0.096383140	0.093145780
				0.2					1.681275000	0.106215200	0.093174570
				0.3					1.681275000	0.115822800	0.093199570
					1.0				1.681275000	0.100200700	0.093047590
					2.0				1.681275000	0.105643700	0.092839790
						0.6			1.681275000	0.096337710	0.093205640
						0.7			1.681275000	0.096292150	0.093248390
							0.2		1.681275000	0.096306760	0.092799840
							0.3		1.681275000	0.096229720	0.092458620
								1.0	1.681275000	0.087711010	0.093686250
								2.0	1.681275000	0.094380540	0.093678310

Table 3: The computed results of skin-friction coefficient, Nusselt and Sherwood numbers for $\beta = 0.5,\ M = 1,\ A = 0.1,\ R = 0.1,\ Pr = 0.7,\ Q = 0.1,\ Nt = 0.1,\ Nb = 0.5$ where a_1=$(1 + We^2 f''^2(0))^{\frac{n-1}{2}}$ and a_2=$(1 + \frac{4}{3}R)$.

Ec	**Sc**	γ	**B**$i1$	**B**$i2$	$-\mathbf{a_1 f''(0)}$	$-\mathbf{a_2}\theta'\mathbf{(0)}$	$\phi'\mathbf{(0)}$
0.1	1.2	1.0	0.1	0.1	1.681275000	0.098130110	0.093177580
0.5					1.681275000	0.103799100	0.092827160
1.0					1.681275000	0.113046500	0.092429350
	1.4				1.433997000	0.098140520	0.093710410
	1.6				1.433997000	0.098149430	0.094138660
		1.5			1.433997000	0.098148540	0.093998040
		2.0			1.433997000	0.098162140	0.094576520
			0.2		1.433997000	0.169395100	0.092967650
			0.3		1.433997000	0.223363000	0.092810330
				0.2	1.433997000	0.097949300	0.175115000
				0.3	1.433997000	0.097787250	0.247730700

The graphs illustrated in this section show the behavior of the velocity, temperature and concentration for the present model in regard to a change in the values of various parameters like n, We, M, R, A, Pr, Q, Nb, Nt, Ec, Sc, $Bi1$ and $Bi2$.

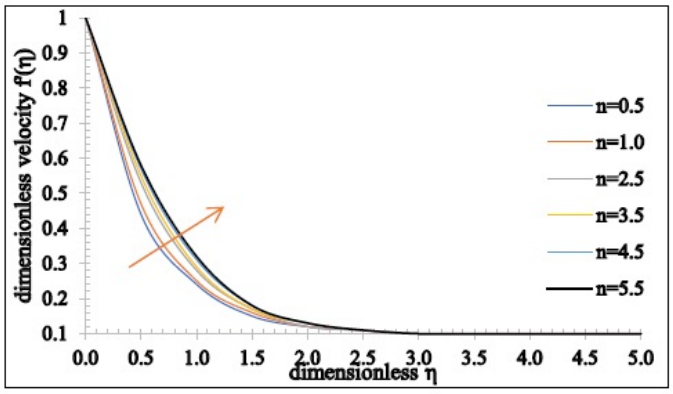

Figure 2: Change in $f'(\eta)$ for values of η

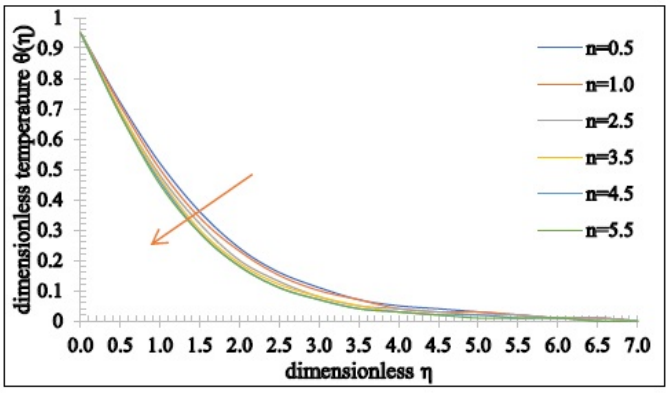

Figure 3: Change in $\theta(\eta)$ for values of η

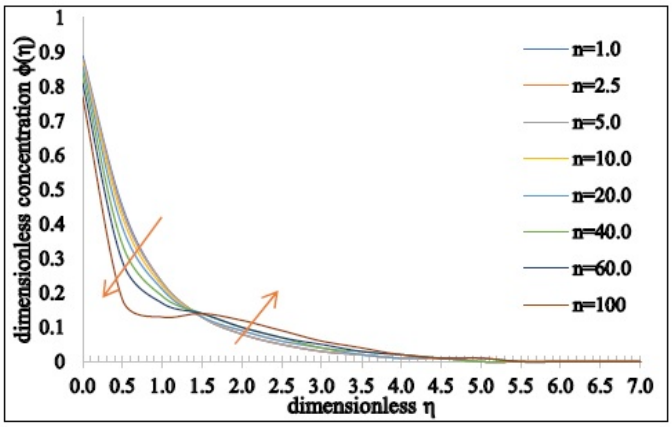

Figure 4: Change in $\phi(\eta)$ for values of η

Figures [2]-[4] are framed to delineate the impact of n on the velocity, temperature and concentration profiles. By enhancing the value of n , velocity field started increased, temperature and concentration distributions can be seen to depress as the larger values of are considered. In addition, a decrement has been observed in the momentum, thermal and concentration boundary layer thickness.

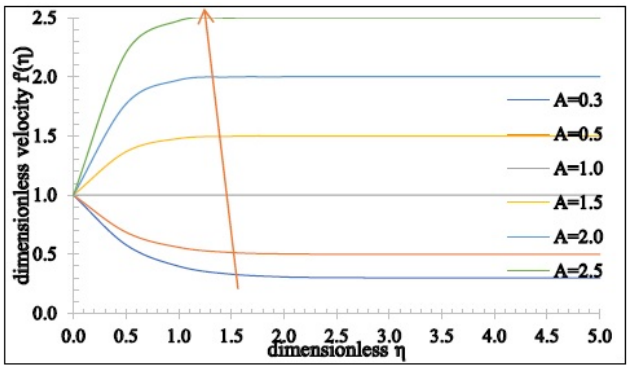

Figure 5: Change in $f'(\eta)$ for values of A

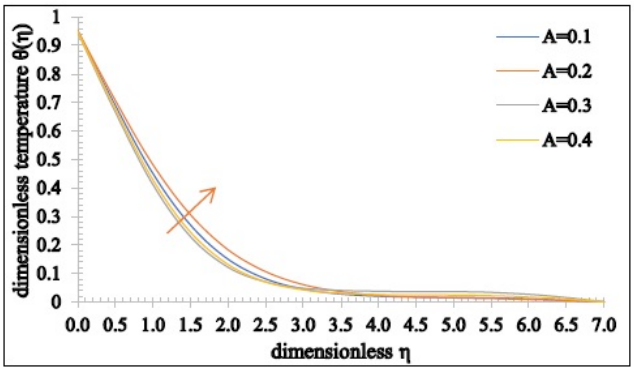

Figure 6: Change in $\theta(\eta)$ for values of A

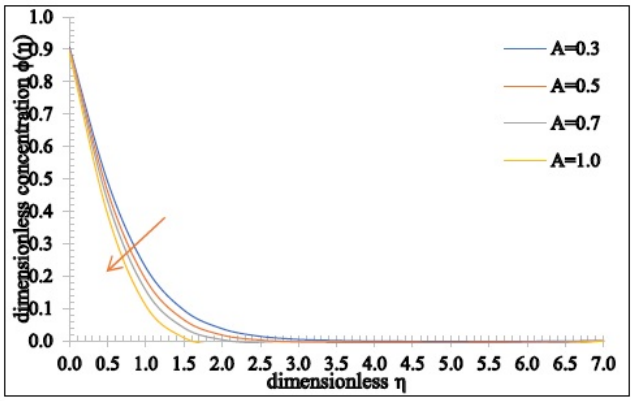

Figure 7: Change in $\phi(\eta)$ for values of A

Figures [5]-[7] are sketched to show the impact of A on the velocity,temperature and concentration distributions. An enhancement in the flow velocity has been observed for $A > 1$. On the other hand, the velocity de-escalates for the case $A < 1$. Also,both the temperature and concentration profiles decrease when A assumes the larger value. As the value of A heightens,the heat transfer from the sheet to the fluid becomes smaller and as a result, the temperature falls. Furthermore,the thermal boundary layer thickness is reduced. Moreover, the concentration boundary layer thickness also shows a declining behavior.

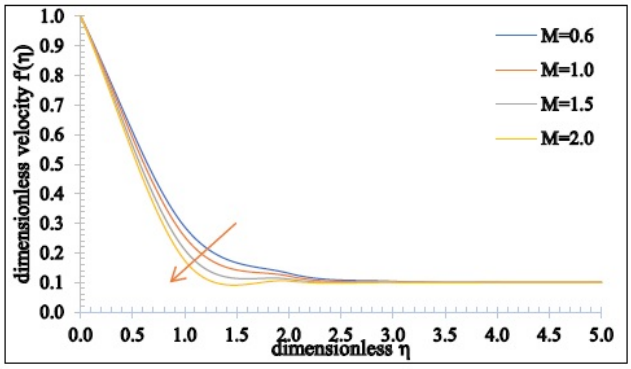

Figure 8: Change in $f'(\eta)$ for values of M

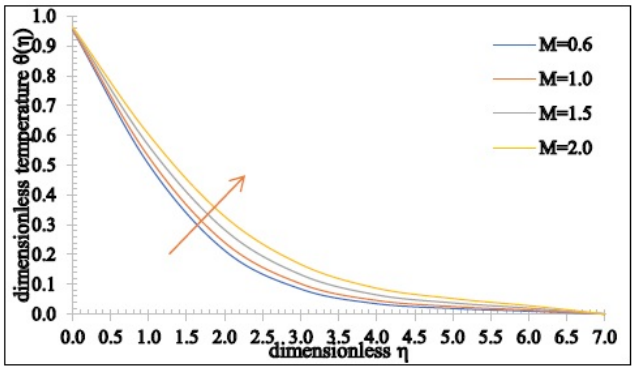

Figure 9: Change in $\theta(\eta)$ for values of M

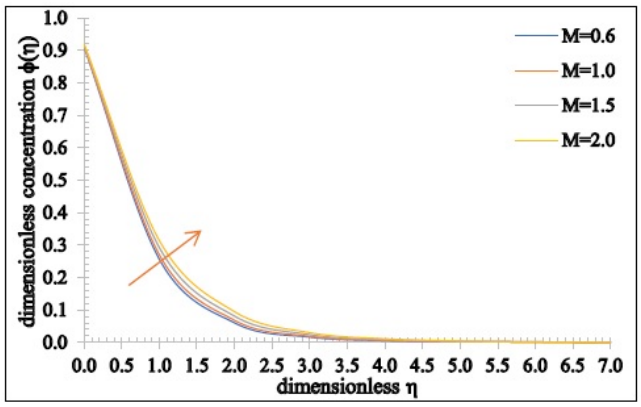

Figure 10: Change in $\phi(\eta)$ for values of M

Figures [8]-[10] represent the impact of the magnetic parameter on the velocity, temperature and concentration profiles. The higher values of M decelerate the velocity and increase the temperature and concentration of the fluid. This stems from the fact that an opposing force is generated by the magnetic field, generally referred as the Lorentz force, which depresses the motion of the fluid resulting in a decrement in the momentum boundary layer thickness and heightens the thermal and concentration boundary layer thickness.

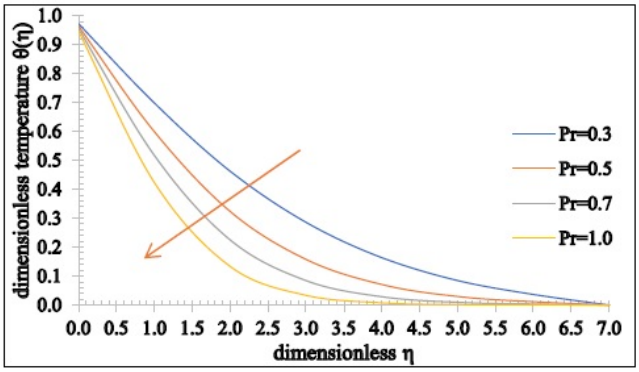

Figure 11: Change in $\theta(\eta)$ for values of P_r

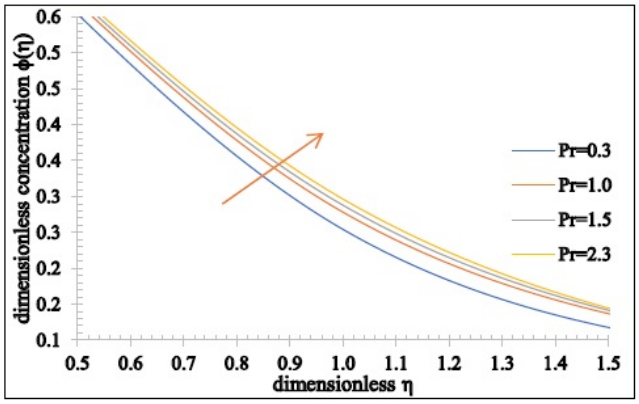

Figure 12: Change in $\phi(\eta)$ for values of P_r

Figures [11]-[12] are framed to delineate the effect of Pr on the temperature and concentration distributions. Since Pr is directly proportionate to the viscous diffusion rate and inversely related to the thermal diffusivity, so the thermal diffusion rate suffers a reduction for the larger estimation of Pr and subsequently, the temperature of the fluid

drops significantly. Moreover, a decrement in the thermal boundary layer thickness has been noted. However, the nanoparticle volume fraction of the fluid can be remarked to escalates for the higher values of Pr . In addition to that, an increment can be seen in the concentration boundary layer thickness.

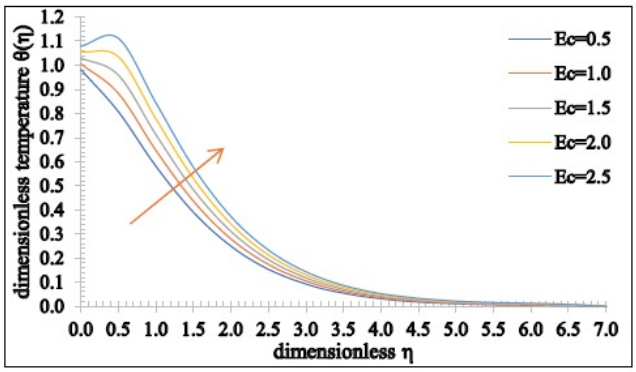

Figure 13: Change in $\theta(\eta)$ for values of E_c

The outcome of Ec on the temperature profile has been characterized through Figure [13]. Physically, the Eckert number depicts the relation between the kinetic energy of the fluid particles and the boundary layer enthalpy. The kinetic energy of the fluid particles rises as Ec assumes the larger values. Hence, the temperature of the fluid climb marginally and therefore, the associated momentum and thermal boundary layer thickness are enhanced.

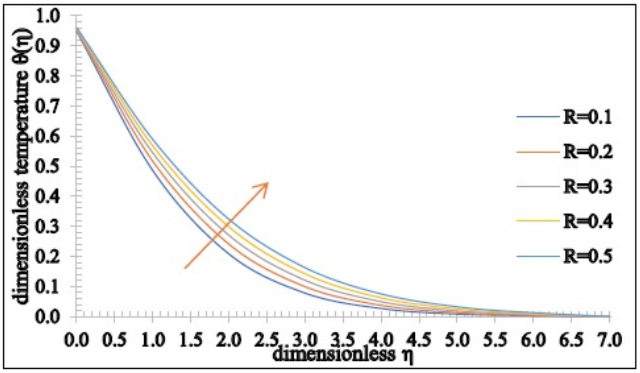

Figure 14: Change in $\theta(\eta)$ for values of R

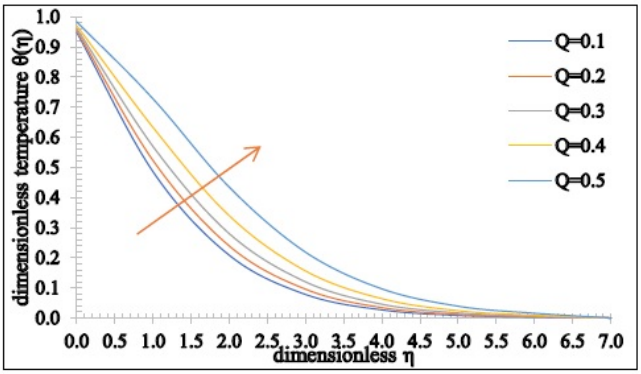

Figure 15: Change in $\theta(\eta)$ for values of Q

Figures [14]-[15] elucidate the effect of the radiation parameter R and the heat generation or absorption parameter

Q on the temperature distributions. Since the heat transfer climbs marginally for the higher estimation of R , thereby an increment in the temperature of the fluid and the thermal boundary layer has been noticed. However, as the value of Q rises, more heat is generated causing an increment in the temperature and the thermal boundary layer thickness. On the other hand, as the value of Q de-escalates, the heat absorbed results in a decrement in the temperature and the associated thermal boundary layer thickness.

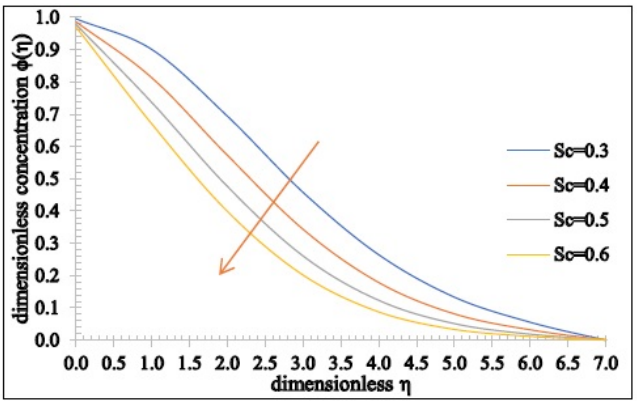

Figure 16: Change in $\phi(\eta)$ for values of Sc

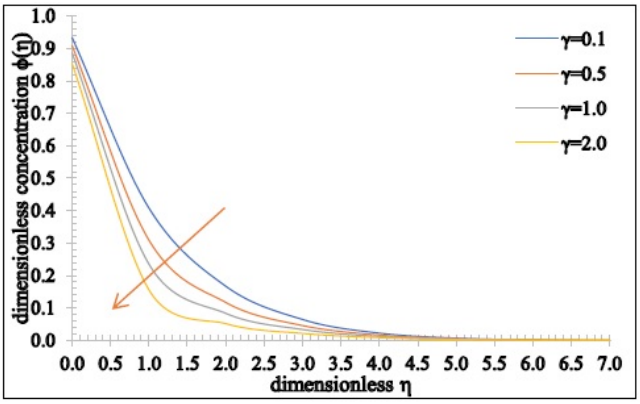

Figure 17: Change in $\phi(\eta)$ for values of γ

Figures [16]-[17] delineate the effect of Sc and γ on the concentration fields. The concentration of the fluid depicts a decreasing behavior as Sc assumes the higher value. This behavior stems from the fact that the Schmidt number and mass diffusion rate have inverse relation, therefore, for the larger Sc , the process of the mass diffusivity slows down and thus, the nanoparticle volume fraction falls, and the concentration boundary layer thickness is reduced. Furthermore, the chemical reaction parameter also has a similar effect on the concentration profile. The larger values of result in a decrement in the chemical molecular diffusion and hence, the concentration of the fluid de-escalates, and the associated concentration boundary layer thickness is reduced.

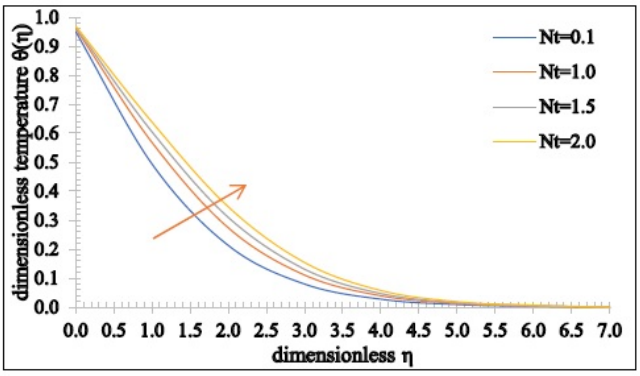

Figure 18: Change in $\theta(\eta)$ for values of Nt

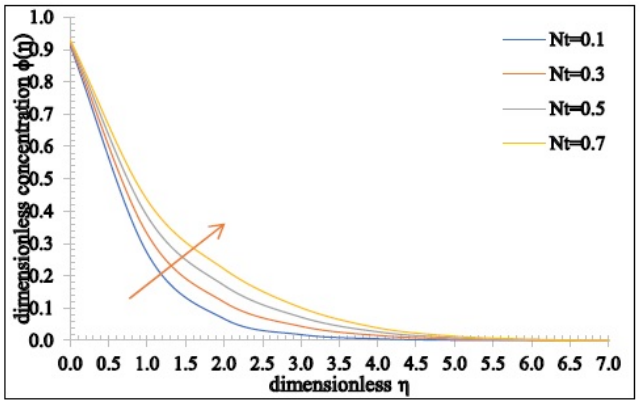

Figure 19: Change in $\phi(\eta)$ for values of Nt

Figures [18]-[19] interpret the impact of the thermophoresis parameter on the temperature and concentration distributions. Both the temperature and concentration escalate by taking larger values of Nt into account. In addition to this, an increment in the associated thermal and concentration boundary layer thickness has been noticed.

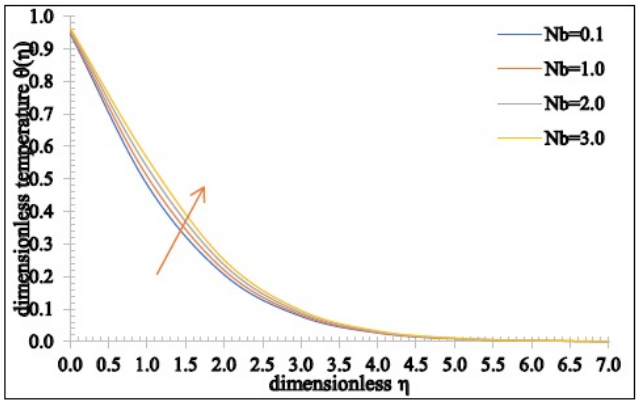

Figure 20: Change in $\theta(\eta)$ for values of Nb

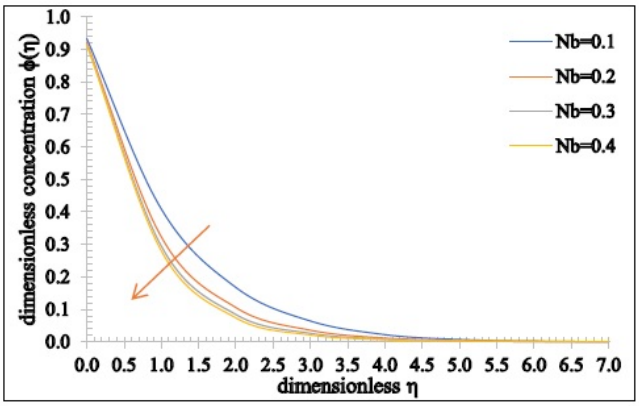

Figure 21: Change in $\phi(\eta)$ for values of Nb

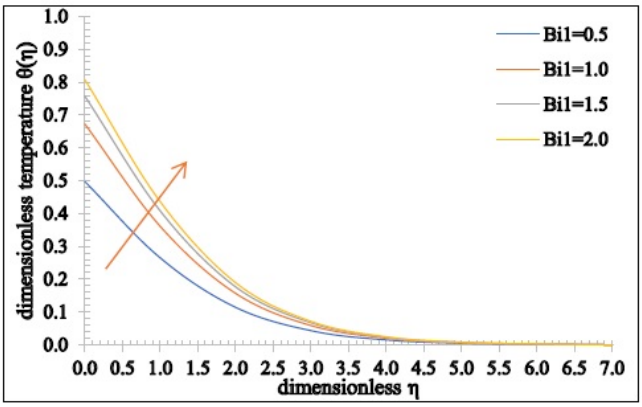

Figure 22: Change in $\theta(\eta)$ for values of $Bi1$

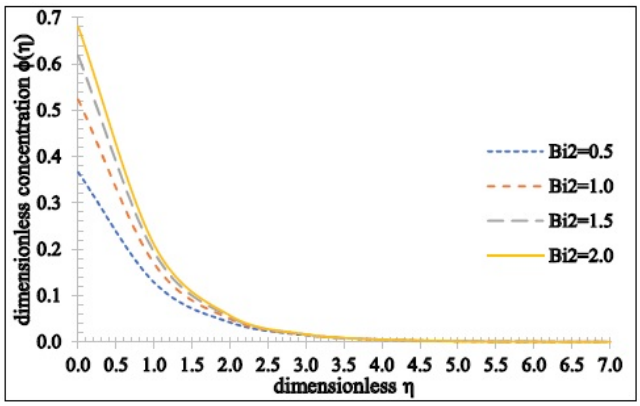

Figure 23: Change in $\phi(\eta)$ for values of $Bi2$

Figures[20]-[21] display the influence of the Brownian motion parameter on the temperature and concentration distributions. The temperature profile climbs marginally for the larger values of Nb. This happens due to the reason that as the value of Nb rises, the movement of the nanoparticles enhances significantly which triggers the kinetic energy of the nanoparticles resulting in an escalation in the temperature and the thermal boundary layer thickness. On the other hand, the concentration of the fluid falls as Nb assumes the higher values. Also, the concentration boundary layer thickness is depressed.

The effect of the thermal Biot number on the temperature distribution and the concentration Biot number on the nanoparticle volume fraction has been portrayed by Figures [22]-[23]. It is remarkable that the temperature can be observed as an increasing function of $Bi1$ the concentration of the fluid also enhances as $Bi2$ heightens. Further to this, the associated thermal and concentration boundary layer thickness are enhanced.

5 Conclusion

We first looked at the work of Dianchen et al. [12] in this preposition and extend edit by counting the viscous discussion and thermal radiation effects. The practices of velocity, temperature and concentration distribution are inspected both graphically by considering different values of different parameters. The significant findings have been listed underneath.The conclusions drawn from the numerical results are summarized below.

Due to the rising values of the magnetic parameter M , the velocity behavior decreases an opposite trend has been observed for the temperature and concentration fields. The temperature falls whereas the concentration escalates for the larger estimation of the Prandtl number in view of the Carreau fluids. The Eckert number accelerates the temperature profile climbs marginally for the Carreau fluid.The heat and mass transfer rates climb significantly as the value of thermophoresis parameter escalates, by considering the Carreau fluids into account. For the Carreau fluids, the heat transfer rate escalates for the radiation parameter.

6 Future recommendations

The problem can also be extended by considering the different fluid models like Williamson, Burger, Jeffery and Tangent hyperbolic nanofluid. The problem can be analyzed by including various other effect like nth-order chemical reaction by taking dust particles. We can also solve the given problem by using different geometries like wedge, channel,cone and cylinder etc. Also, apply the higher order finite elements in space and the Galerkin discretization scheme for temporal discretization.

Acknowledgment

Help by **Prof. S R Koneru,** Retd. Professor, Department of Mathematics, IIT Mumbai in the preparation of this paper is gratefully acknowledged.

References

[1] N.S. Akbar, S. Nadeem, R.U. Haq and Z.H. Khan, *Radiation effects on MHD stagnation point flow of nanofluid towards a stretching surface with convective boundary condition*, Chinese J. Aeronautics **26** (2013), no. 6, 1389–1397.

[2] N.S. Akbar, S. Nadeem and Z.H. Khan, *Numerical simulation of peristaltic flow of a Carreau nanofluid in an asymmetric channel*, Alexandria Engin. J. **53** (2014), no. 1, 191–197.

[3] S.U.S. Choi, *Nanofluid technology: current status and future research* , Tech. Rep. ANL/ET/CP-97466, Argonne National Lab. (ANL), Argonne, IL (United States), 1998, Oct. 20, pp. 1–21.

[4] R. Ellahi, A. Riaz, S. Nadeem and M. Ali, *Peristaltic flow of Carreau fluid in a rectangular duct through a porous medium*, Math. Prob. Engin. **2012** (2012).

[5] M. Farooq, M.I. Khan, M. Waqas, T. Hayat, A. Alsaedi and M.I. Khan, *MHD stagnation point flow of viscoelastic nanofluid with non-linear radiation effects*, J. Molecular Liq. **221** (2016), 1097–1103, 201.

[6] K. Govardhan, G. Narender and G. Sreedhar Sarma, *Viscous dissipation and chemical reaction effects on MHD Casson nanofluid over a stretching sheet*, Malay. J. Fund. Appl. Sci. **15** (2019), no. 4, 585–592.

[7] R.U. Haq, S. Nadeem, Z.H. Khan, and N.S. Akbar, *Thermal radiation and slip effects on MHD stagnation point flow of nanofluid over a stretching sheet*, Phys. E: Low-dimensional Syst. Nanostruct. **65** (2015), 17–23.

[8] T. Hayat, F.M. Abbasi, B. Ahmad and A. Alsaedi, *Peristaltic transport of Carreau-Yasuda fluid in a curved channel with slip effects*, PloS One **9** (2014), no. 4, e95070.

[9] T. Hayat, N. Saleem and N. Ali, *Effect of induced magnetic field on peristaltic transport of a Carreau fluid*, Commun. Nonlinear Sci. Numer. Simul. **15** (2010), no. 9, 2407–2423.

[10] T. Hayat, I. Ullah, B. Ahmad and A. Alsaedi, *Radiative flow of Carreau liquid in presence of Newtonian heating and chemical reaction*, Results Phys. **7** (2017), 715–722.

[11] A. Ishak, K. Jafar, R.A. Nazar and L. Pop, *MHD stagnation point flow towards a stretching sheet*, Phys. A: Statist. Mech. Appl. **388** (2009), no. 17, 3377–3383.

[12] D. Lu, M. Ramzan, N.U. Huda, J.D. Chung and U. Farooq, *Nonlinear radiation effect on MHD Carreau nanofluid flow over a radially stretching surface with zero mass flux at the surface*, Sci. Rep. **8** (2018), no. 1, 3709.

[13] F. Mabood, S. Shateyi, M. Rashidi, E. Momoniat and N. Freidoonimehr, *MHD stagnation point flow heat and mass transfer of nanofluids in porous medium with radiation, viscous dissipation and chemical reaction*, Adv. Powder Technol. **27** (2016), no. 2, 742–749.

[14] T.R. Mahapatra and A.S. Gupta, *Heat transfer in stagnation-point flowtowards a stretching sheet*, Heat Mass Transfer **38** (2002), no. 6, 517–521.

[15] G. Narender, K. Govardhan and G. Sreedhar Sarma, *Magnetohydrodynamic stagnation point on a Casson nanofluid flow over a radially stretching sheet*, Beilstein J. Nanotechnol. **11** (2020), 1303—1315.

[16] R. Nazar, N. Amin, D. Filip and L. Pop, *Stagnation point flow of a micropolar fluid towards a stretching sheet*, Int. J. Non-Linear Mech. **39** (2004), no. 7, 1227–1235.

[17] A. Raptis, C. Perdikis and H.S. Takhar, *Effect of thermal radiation on MHD flow*, Appl. Math. Comput. **153** (2004), no. 3, 645–649.

[18] C.Sulochana, G. P. Ashwinkumar, and N. Sandeep, *Transpiration effect on stagnation-point flow of a Carreau nanofluid in the presence of thermophoresis and Brownian motion*, Alexandria Engin. J. **55** (2016), no. 2, 1151–1157.

[19] S. Suneetha and K. Gangadhar, *Thermal radiation effect on MHD stagnation point flow of a Carreau fluid with convective boundary condition*, Open Sci. J. Math. Appl. **3** (2015), no. 5, 121.

[20] M. Waqas, M. Alsaedi, S. A. Shehzad, T. Hayat and S. Asghar, *Mixed convective stagnation point flow of Carreau fluid with variable properties*, J. Brazil. Soc. Mech. Sci. Engin. **39** (2017), no. 8, 3005–3017.